ELSEVIER

Journal of Fluids and Structures 26 (2010) 900–917

JOURNAL OF FLUIDS AND STRUCTURES

www.elsevier.com/locate/jfs

Effect of novel synthetic jet on wake vortex shedding modes of a circular cylinder

Li Hao Feng, Jin Jun Wang*, Chong Pan

Fluid Mechanics Institute, Beijing University of Aeronautics and Astronautics and Fluid Mechanics Key Laboratory of Education Ministry, Beijing 100191, PR China

Received 22 November 2009; accepted 27 May 2010
Available online 8 July 2010

Abstract

A novel actuator signal achieved by changing the ratio of the suction duty cycle to the blowing duty cycle is adopted to enhance the control effect of the synthetic jet for the flow around a circular cylinder. The suction duty cycle factor k defined as the ratio between the time duration of the suction cycle and the blowing cycle and the equivalent momentum coefficient C_μ are introduced as the determining parameters. The synthetic jet is positioned at the rear stagnation point in order to introduce symmetric perturbations upon the flow field. The proper orthogonal decomposition (POD) technique is applied for the analysis of the spanwise vorticity field. Increasing the suction duty cycle factor, the momentum coefficient is enhanced, and thus a stronger and larger scale synthetic jet vortex pair with a higher convection velocity is generated. The synthetic jet vortex pair interacts with the spanwise vorticity shear layers behind both sides of the cylinder, resulting in the variations of the wake vortex shedding modes at $\mathrm{Re} = 950$: for $k = 0.25$, $C_\mu = 0.148$, vortex synchronization at the subharmonic excitation frequency with antisymmetric shedding mode; for $0.50 \le k \le 1.00$, $0.213 \le C_\mu \le 0.378$, vortex synchronization at the excitation frequency with the symmetric or antisymmetric shedding modes; for $2.00 \le k \le 4.00$, $0.850 \le C_\mu \le 2.362$, vortex synchronization at the excitation frequency with symmetric shedding mode. Hence, the control effect of the synthetic jet upon the wake vortex of a circular cylinder can be enhanced by increasing the suction duty cycle factor so as to increase the momentum coefficient. This is also validated at a higher Reynolds number $\mathrm{Re} = 1600$.

Keywords: Synthetic jet; Novel actuator signal; Circular cylinder; Proper orthogonal decomposition (POD); Shedding mode; Vortex synchronization

1. Introduction

The subject of flow control has drawn considerable attention for its broad engineering applications. Generally, it can be broadly categorized into passive and active control methods (Choi et al., 2008; Jukes and Choi, 2009a). Active control methods are usually more convenient than passive methods, since they can be adjusted to attain the optimum effect during the control process and be turned off if not needed. In the 1990s, the synthetic jet actuator was developed in the laboratory (Ziada, 1995; Smith and Glezer, 1998) based on the observation of zero-net-mass-flux jets by Ingard

*Corresponding author. Tel.: +86 10 8233 9304; fax: +86 10 8232 8501.
E-mail address: jjwang@buaa.edu.cn (J.J. Wang).

0889-9746/$ - see front matter © 2010 Elsevier Ltd. All rights reserved.
doi:10.1016/j.jfluidstructs.2010.05.003

and Labate (1950). After that, the synthetic jet has become a hot topic as a kind of active control method due to its unique advantages. It has been widely applied in various fields, including the modification of the aerodynamic characteristics of bluff bodies, control of lift and drag on airfoils and air vehicles, reduction of skin friction of a flat-plate boundary layer, mixing in circular jets, and control of internal flow separation and of cavity oscillations (Glezer and Amitay, 2002; Zhang et al., 2008).

The synthetic jet was first used as a separation control method to control the boundary layer separation of a circular cylinder by Amitay et al. (1997). In their experiment, synthetic jets were issued from a pair of slots with the jet exit angle varied from 0° to 180°. They indicated that the interaction of synthetic jets with an embedding flow led to the formation of closed recirculation regions, which enabled an apparent modification of the flow boundary. Further surface pressure measurement demonstrated that the synthetic jets could reduce drag up to 30%. After that, many researchers have proved that the synthetic jet can efficiently delay separation of the circular cylinder, make the separation region diminish or even completely disappear, lead to a drag reduction, and reduce resonant response (Amitay et al., 1998; Crook et al., 1999; Béra et al., 2000; Tensi et al., 2002; Fujisawa and Takeda, 2003; Glezer et al., 2003; Wolfe and Ziada, 2003; Fujisawa et al., 2004; Wang et al., 2007; Feng et al., 2008). Glezer et al. (2003) indicated that a series of discrete vortices were generated over the circular cylinder surface interacting with the wall boundary layers, which led to the modification of the surface pressure distribution and the delay of the separation point. However, most of the previous investigations paid less attention to the variations of the vortex structures around the circular cylinder, which we deduce should play an important role in separation delay and drag reduction.

According to Lucor and Karniadakis (2004), the dominant vortex patterns of an oscillating cylinder can be categorized into 2S, 2P and P+S modes. A 2S shedding mode implies that in each half-cycle of the oscillation a single vortex sheds into the wake. A 2P shedding mode means that in each half-cycle a pair of vortices of opposite sign sheds into the wake. Finally, a P+S mode is an asymmetric version of the 2P mode where a pair of vortices of opposite sign and a single vortex shed downstream in each cycle. Adopting this classification, the standard Karman vortex is equivalent to a 2S mode. The above-mentioned three modes are all antisymmetric shedding modes. Besides, there is a symmetric shedding mode, where a pair of vortices is shedding in phase from both sides of the circular cylinder during one cycle. Ongoren and Rockwell (1988), Liu and Fu (2003), Nishihara et al. (2005), Xu et al. (2006), Konstantinidis and Balabani (2007) and Jukes and Choi (2009b) all observed the existence of the symmetric vortex shedding mode by means of cylinder oscillations, free-stream perturbations or symmetric perturbations imposed at both the upper and bottom separation points. The symmetric shedding mode is potential of engineering significance and should be given special attention, since this flow structure leads to zero mean and fluctuating lift on the cylinder (Xu et al., 2006).

Vortex shedding behind a bluff body displays complicated spatio-temporal variations that can be analyzed using proper orthogonal decomposition (POD). POD as a statistical technique allows us to present coherent structures as a low-dimensional description of the flow (Dipankar et al., 2007). For detailed descriptions of the POD method refer to the introduction papers by Berkooz et al. (1993) and Hilberg et al. (1994). Since lower POD modes usually represent the large-scale coherent structures that dominate the global flow field and occupy most of energy, we can extract the dominant shedding mode by analyzing lower POD modes. Besides, the global flow field can be reconstructed based on the first few modes, in order to eliminate the small-scale turbulent structures and background noises. The POD technique has already been used by Ma et al. (2000, 2003), Dipankar et al. (2007) and Konstantinidis et al. (2007) for the analysis of the flow around a circular cylinder. Recently, Epps and Techet (2009) applied this technique to study the reverse Karman vortex of a live swimming fish, and suggested a threshold criterion that could be used as a rough limit of the validity of POD modes extracted from experimental data.

In the application of the synthetic jet, it is required to increase the efficiency of the synthetic jet control. Shuster and Smith (2004) and Holman et al. (2005) discussed the criterion condition to form a synthetic jet based on the "slug" model proposed by Smith and Glezer (1998). They suggested that the formation of the synthetic jet is governed by the self-induced velocity V_I of the vortex formed during the blowing cycle and the average suction velocity V_S during the suction cycle. By order of magnitude analysis they deduced the theoretical jet formation criterion as

$$\frac{V_I}{V_S} > K, \tag{1}$$

where the constant K is approximately 2 and 0.16 for two-dimensional and axisymmetric synthetic jets, respectively. Eq. (1) suggests that the condition for the synthetic jet formation is that the ratio of the self-induced velocity of the vortex to the averaged suction velocity should be larger than the constant K.

Therefore, if the time scale of the suction cycle increases and the blowing cycle decreases, while the mass flux stays the same over the two cycles, the blowing velocity will be enhanced while the suction velocity will be reduced. In this case, it is expected that the vortex formed during the blowing cycle has a larger convection speed, and the entrainment of the orifice during the suction cycle on the vortex is reduced. Based on this consideration, Zhang and Wang (2007) proposed

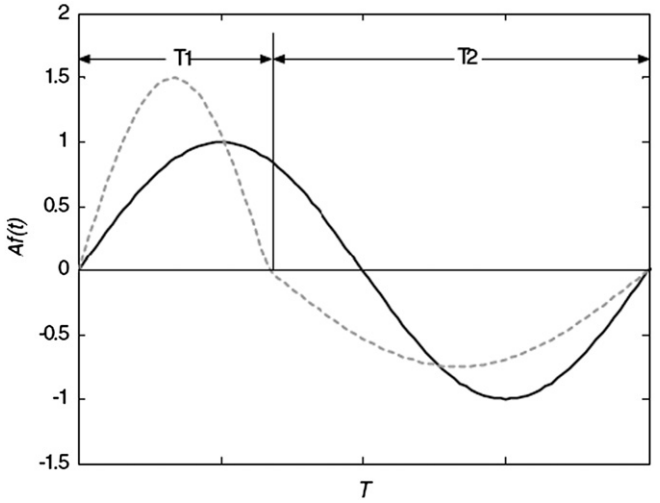

Fig. 1. Novel actuator signal wave pattern. The x coordinate is the time and the y coordinate is the velocity magnitude (Zhang and Wang, 2007).

a novel actuator signal to generate a more efficient synthetic jet. It was a standard sinusoidal function with some modulation, as shown in Fig. 1. In this novel actuator signal, T_1 and T_2 represent the time duration of the blowing cycle and the suction cycle in one period, respectively. The ratio of these two parameters is defined as the suction duty cycle factor $k = T_2/T_1$. According to this definition, $k>1$ means that the suction cycle is longer than the blowing cycle, and thus the averaged suction velocity will be less than the averaged blowing velocity, while $k<1$ causes an opposite result.

Zhang and Wang (2007) numerically proved that the entrainment effect of the actuator decreased with the increase of the suction duty cycle factor k. Thus the vortex pair could propagate farther downstream and coalesce to synthesize a stronger one. Feng et al. (2008) primarily proved that this novel actuator signal could substantially enhance the effect of the circular cylinder separation control with the synthetic jet positioned at the rear stagnation point, using the hydrogen bubble flow visualization technique. Recently, Shan and Wang (2010) investigated the influence of the novel actuator signal on an axisymmetric synthetic jet by using flow visualization and particle image velocimetry (PIV) techniques. It was found that the vortex rings were more likely to form when increasing the suction duty cycle factor.

In the present work, flow around a circular cylinder controlled by a synthetic jet adopting a novel actuator signal is experimentally investigated by PIV measurements. The synthetic jet is positioned at the rear stagnation point in order to introduce symmetric perturbations upon the near wake region. Variations of the wake vortex shedding mode are given particular attention by means of the POD technique, in order to validate the improvement of the control effect when applying the novel actuator signal.

2. Experimental details

2.1. Novel synthetic jet actuator system

The novel synthetic jet actuator system comprised a computer, an A/D conversion card, a programmable logic controller (PLC), a servo electromotor, a center-setting crank mechanism which was formed by an eccentric disk and a connecting rod, a piston, and an 'L'-shape hollow cylinder (Fig. 2). The computer was connected to the PLC with the A/D card. The PLC controlled the servo electromotor, which was connected to the piston inside the vertical section of the 'L'-shape hollow cylinder with the center-setting crank mechanism. A slot was disposed on the external surface of the horizontal section of the 'L'-shape hollow cylinder and paralleled to its axis. The novel actuator signal could be programmed in the computer, and then it was stored in the PLC by the A/D card. Thus the PLC could control the servo electromotor to do circular motion according to the designed signal. The circular motion of the servo electromotor was transferred to a come-and-go motion with quick-return characteristic of the piston. Meanwhile, the fluid inside the cavity would be injected and sucked from the slot, and thus the synthetic jet vortex pair was generated. The generation

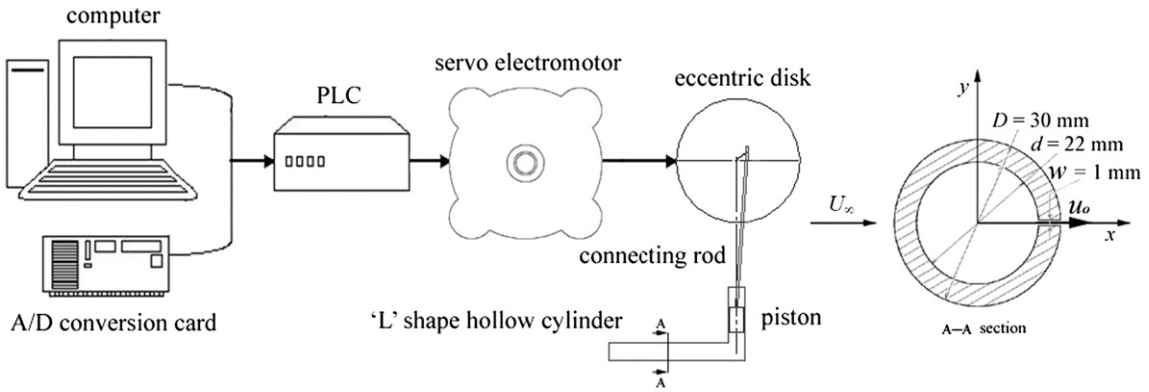

Fig. 2. Schematic of the novel synthetic jet actuator system.

cycle and exit velocity of the synthetic jet were altered by adjusting the eccentric disk amplitude A, the excitation frequency f_e and the suction duty cycle factor k.

The experiment was conducted in a recirculation water channel. The size of the test section is $600 \times 600 \times 4800$ mm, and the streamwise turbulence intensity is no more than 0.8%. The experimental model was the horizontal section of the 'L'-shape hollow cylinder with outer diameter $D = 30$ mm, inner diameter $d = 22$ mm and length 600 mm (Fig. 2). The origin of the coordinate system is located at the center of the experimental cylinder, while the x and y axes represent the streamwise and transverse directions, respectively. The vertical section of the 'L'-shape hollow cylinder had an outer diameter 30 mm and inner diameter 24 mm. The piston inside the hollow cylinder also had an outer diameter $D_p = 24$ mm.

One end-plate with height $20D$, length $50D$ and thickness 10 mm was vertically mounted across the experimental circular cylinder and had a distance of $3D$ from the inner wall of the test section. It had a 4:1 elliptical leading edge to avoid flow separation, which was $10D$ from the experimental cylinder center. The other end of the experimental cylinder was secured on the outer wall of the water channel directly, and no end plate was used in this end to avoid any additional light reflection when using the CCD camera. The test section was in the very-near wake region, about $8.33D$ from both the inner end plate and outer wall. Since the flow was kept laminar, the thickness of the boundary layer developing on the outer end of the circular cylinder was no more than $0.5D$. Thus it would not have a strong influence on the test section (Konstantinidis and Balabani, 2007).

The slot, with a width $w = 1$ mm and a spanwise length $l = 50$ mm, was in the mid-span region of the test-section and fixed at the rear stagnation point. This configuration is similar with that of Abdou and Ziada (2006), who used a pair of loudspeakers mounted on each side of the hollow cylinder as the driver to produce a high-aspect-ratio synthetic jet with the aspect ratio up to several hundreds. In contrast, in order to ensure a well developed two-dimensional synthetic jet flow, the length of the present slot was selected no more than $1.67D$ due to the different pipe system. However, as mentioned above, the present work focused on the very-near wake region of the cylinder in the mid-span of the slot. The three-dimensional effect introduced by the ends of the synthetic jet flow would not have a crucial influence. This has been confirmed in the previous work by Feng et al. (2008), which indicated that the influenced wake flow by a $1.67D$ synthetic jet was kept two-dimensional very well in the near wake.

2.2. Experimental parameters

According to Zhang and Wang (2007), the synthetic jet exit velocity has the following forms when adopting the novel actuator signal:

$$u_0(t) = \frac{k+1}{2} U_0 \sin\left(2\pi f_e \frac{k+1}{2}(t-nT)\right), \quad nT \le t \le nT + \frac{T}{k+1}, \tag{2}$$

$$u_0(t) = \frac{k+1}{2k} U_0 \sin\left(2\pi f_e \frac{k+1}{2k}(t-nT) + \frac{k-1}{k}\pi\right), \quad nT + \frac{T}{k+1} \le t \le (n+1)T, \tag{3}$$

where $T = 1/f_e$ is the actuator oscillation cycle, t is the excitation time and U_0 is the time-averaged exit velocity amplitude when the suction duty cycle factor k is 1. The velocity amplitude U_0 can be calculated based on mass

conservation:

$$U_0 = \frac{\pi^2 D_p^2}{2lw} A f_e. \tag{4}$$

According to Smith and Glezer (1998), the synthetic jet exit velocity is usually evaluated by the time-averaged blowing velocity during one cycle:

$$\overline{U_0} = \frac{1}{T}\int_0^{\frac{T}{k+1}} u_0(t)dt = \frac{U_0}{\pi}. \tag{5}$$

However, the influence of the suction duty cycle factor k is not manifested by the above definition, since it is a time-averaged processing procedure over the whole cycle. Here, the blowing velocity averaged only over the blowing cycle is calculated as follows:

$$\overline{U_b} = \frac{1}{T/(k+1)}\int_0^{\frac{T}{k+1}} u_0(t)dt = \frac{k+1}{\pi} U_0. \tag{6}$$

As can be seen from the above equation, the suction duty cycle factor k has a significant influence on the exit velocity, suggesting that a higher blowing velocity is achieved with a larger k. Hence, the time-averaged blowing velocity during the blowing cycle is adopted in order to manifest the influence of k. Besides, the jet momentum coefficient is a key parameter for characterizing jet interaction with the external cross-flow. It is defined as the ratio of the synthetic jet momentum flux to the free-stream momentum flux (Amitay et al., 1997, 1998; Tensi et al., 2002):

$$C_\mu = 2\left(\frac{\overline{U_b}}{U_\infty}\right)^2 \left(\frac{w}{D}\right). \tag{7}$$

The main part of the experiment was conducted at a free-stream velocity of $U_\infty = 41.8$ mm/s, corresponding to the circular cylinder Reynolds number Re = 950. For this Reynolds number, the actuator amplitude A and the excitation frequency f_e were fixed at 5.5 mm and 0.50 Hz, respectively, while the suction duty cycle factor k was selected at 0.25, 0.50, 1.00, 2.00 and 4.00. The exit jet velocity for these cases is presented in Fig. 3 based on Eqs. (2)–(4). It is indicated that the wave form of the exit velocity changes thoroughly with the suction duty cycle factor k, such as the equivalent momentum coefficient C_μ, which was 0.148, 0.213, 0.378, 0.850 and 2.362, respectively. In order to further validate the control effect of the novel synthetic jet, a higher Reynolds number at Re = 1600 with k selected at 1.00 and 4.00 was

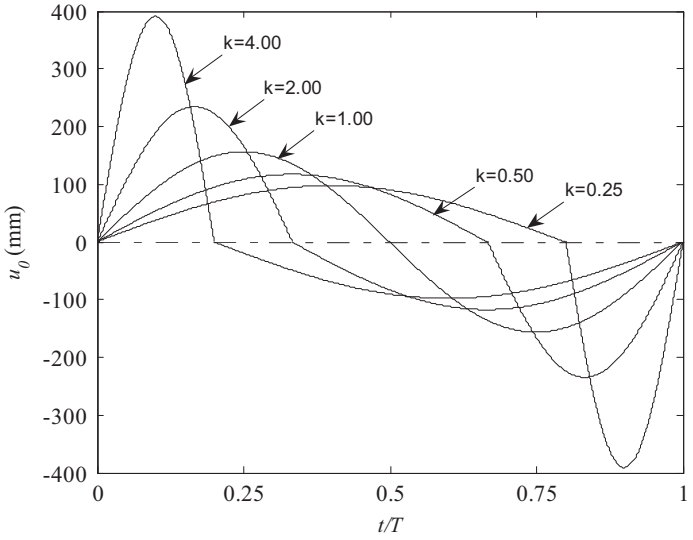

Fig. 3. Exit velocity of the synthetic jet for different suction duty cycle factors.

also tested, corresponding to the momentum coefficient $C_\mu = 0.129$ and 0.807, respectively. In the following, the main results were obtained at Re = 950, unless Re = 1600 is specifically mentioned. The suction duty cycle factor k is used as a parameter to characterize the actuator signal for the generation of the novel synthetic jet, while the equivalent momentum coefficient C_μ is introduced as the determining parameter for comparison between the synthetic jet output and the free stream.

2.3. Particle image velocimetry

The flow field was measured by the PIV technique. The field of view was illuminated by a light sheet from a Nd:YAG successive laser. The tracer particles were hollow glass beads with average diameter 5 μm and density 1.05 g/mm^3. The test-section was captured by a high speed CCD camera having a spatial resolution of 640 × 480 pixels with 8 bits in gray level. Due to the resolution of the CCD, it had a range of $0 \le x/D \le 3$ and $-1 \le y/D \le 1$. This size of view was enough, since the present work focused on the near-wake vortex evolution of the cylinder. The sampling frequency of the high speed CCD was 100 Hz with the exposure time 5 ms. Ten thousands frames were recorded continuously in one case. The images were dealt using the gray-level difference algorithm for the cross-correlation calculation between two successive images. Gaussian peak fit was applied to enhance the resolution of cross-correlation peak identification to a sub-pixel level. The sizes of the interrogation window and search window were set to 16 × 16 pixels and 8 × 8 pixels, respectively. Multi-grid iteration with window deformation was also used to improve the trace accuracy of the interrogation window. Ultimately, the absolute uncertainty in measured velocity would be better than 2 mm/s.

3. Results and discussion

3.1. Evolution of synthetic jet vortex pair

In order to investigate the influence of the novel actuator signal on the synthetic jet, evolution of the phase-averaged spanwise vorticity $\langle \omega_z \rangle D/U_\infty$, where $\omega_z = \partial v/\partial x - \partial u/\partial y$, of the synthetic jet is shown in Fig. 4. The phase-averaging method follows Zhou and Yiu (2006) and Kim et al. (2006). The reference signal is selected near the rear stagnation point at $x/D = 0.6$, $y/D = 0$. Phase $t = 0$ is defined as the start of the blowing cycle of the synthetic jet. It is shown that a stronger and larger scale synthetic jet vortex pair forms and the vortex pair can propagate farther downstream when increasing the suction duty cycle factor, which is in good agreement with the simulation results of Zhang and Wang (2007). It is noteworthy that the wake vortex of the circular cylinder has also been affected by the synthetic jet vortex pair. It seems that the wake vortex sheds downstream with a nearly symmetric mode accompanying with the synthetic jet vortex pair. However, the phase-averaged results in Fig. 4 might not display the real evolution information for the wake vortex, since the reference signal of the present phase average is selected near the exit. It can well characterize the evolution of the synthetic jet vortex pair, while it may not be suitable for the phase average of the wake vortex, especially when the wake vortex is not synchronized by the synthetic jet. This issue will be illustrated in the following.

The vortex centroid method is adopted to detect the synthetic jet vortex center (Cantwell and Coles, 1983; Sung and Yoo, 2003; Konstantinidis et al., 2005; Kim et al., 2006), in order to obtain the quantitative characteristics of the evolution of the synthetic jet vortex affected by the novel actuator signal. Briefly, the circulation Γ can be obtained by the integration of the vorticity field above a given threshold, and then the vortex center x_c and y_c can be calculated from the equivalent vortex centroid by regarding the distribution of vorticity as that of density.

Fig. 5 shows the evolution of the circulation $|\Gamma/U_\infty D|$ for the synthetic jet vortex. The integration is performed only for values of $\omega_z/\omega_{zp} \ge 0.5$, where ω_{zp} is the local peak of the vorticity, to avoid relative noisy data according to Sung and Yoo (2003) and Kim et al. (2006). Only the vortices developing in the region $y/D \ge 0$ are analyzed due to the symmetry of the flow field, corresponding to the positive synthetic jet vortices. It is indicated that the circulation of the synthetic jet vortex at different suction duty cycle factors increases to a maximum and then gradually decreases to nearly zero. Comparing with the case of $k = 1.00$, $C_\mu = 0.378$, the circulation is weakened less when decreasing k to 0.50 and 0.25, i.e. C_μ to 0.213 and 0.148, respectively; in contrast, the circulation is enhanced extremely when increasing k to 2.00 and 4.00, i.e. C_μ to 0.850 and 2.362, respectively.

Fig. 6 shows the streamwise and transverse trajectories of the synthetic jet vortex. It is indicated that the synthetic jet vortex pair could propagate a further streamwise and transverse downstream position as the suction duty cycle factor increases. The streamwise and transverse trajectories have a higher slope at a larger suction duty cycle factor, indicating

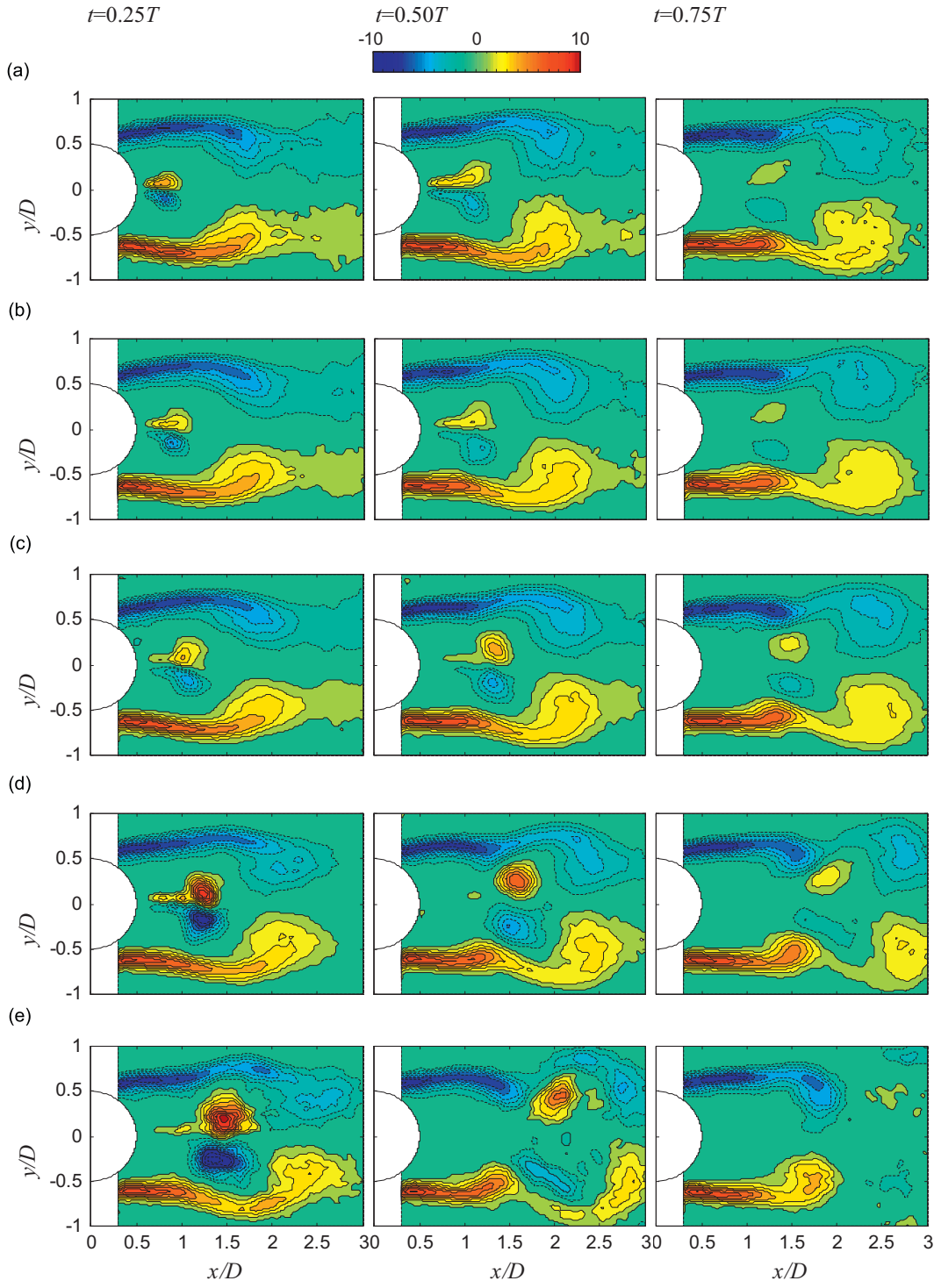

Fig. 4. Evolution of the phase-averaged synthetic jet vortex pair at different suction duty cycle factors at Re = 950, where $T = 2.00$ s is the time duration of one cycle, $t = 0$ is defined as the start of the blowing cycle: (a) $k = 0.25$, $C_\mu = 0.148$; (b) 0.50, 0.213; (c) 1.00, 0.378; (d) 2.00, 0.850; and (e) 4.00, 2.362. Contour levels: ± 1.

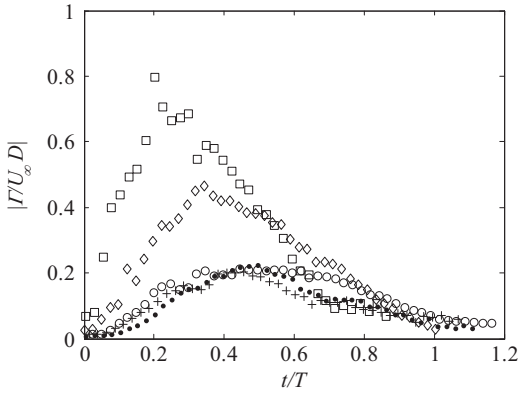

Fig. 5. Evolution of the circulation $|\Gamma/U_\infty D|$ for the synthetic jet vortex at different suction duty cycle factors at Re = 950: ●, $k = 0.25$, $C_\mu = 0.148$; +, 0.50, 0.213; ○, 1.00, 0.378; ◇, 2.00, 0.850; and □, 4.00, 2.362.

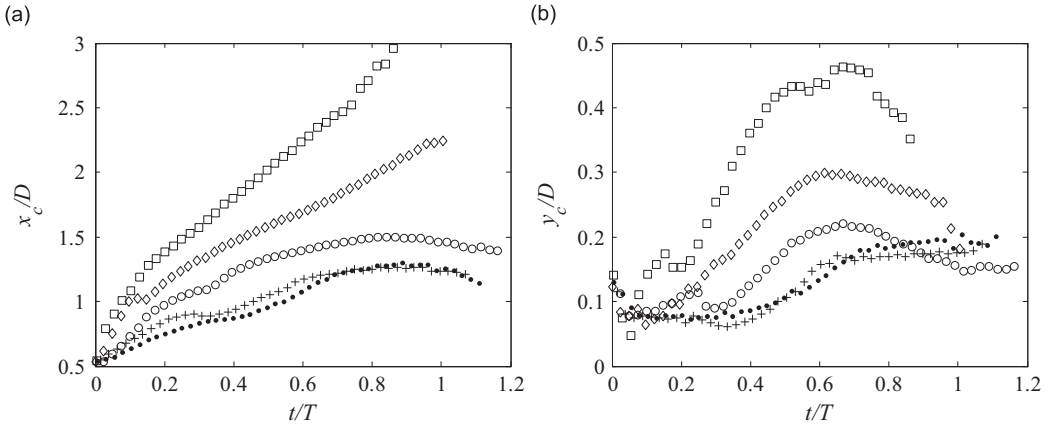

Fig. 6. Trajectory of the synthetic jet vortex at different suction duty cycle factors at Re = 950: (a) streamwise trajectory and (b) transverse trajectory. Symbols are same as Fig. 5.

that both the streamwise and transverse convection velocities of the synthetic jet vortex increase with the suction duty cycle factor k as well as the momentum coefficient C_μ.

3.2. Power spectrum analysis

Fig. 7 shows power spectrum of the spanwise vorticity $\omega_z D/U_\infty$ at $x/D = 3$, $y/D = 0.6$ for all cases. For the natural case (Fig. 7(a)), the power spectrum indicates that the dominant Karman vortex shedding frequency is 0.30 Hz, corresponding to St = 0.215. When adopting the standard sinusoidal actuator signal, namely $k = 1.00$, $C_\mu = 0.378$ (Fig. 7(d)), there exists a peak 0.50 Hz, suggesting that the vortex shedding is dominated by the synthetic jet. When decreasing the suction duty cycle factor k to 0.50 and the momentum coefficient C_μ to 0.213 (Fig. 7(c)), the power spectrum peak becomes 0.49 Hz. It is worth noticing that, when adopting the novel actuator signal, there is a time delay between the blowing and suction cycles inevitably. The time delay is less than 0.05 s, which leads to an uncertainty range no more than 0.01 Hz. Therefore, the difference between 0.49 and 0.50 Hz can be considered in this range. Thus, Fig. 7(c) suggests that the synthetic jet could dominate the wake vortex shedding. For $k = 0.25$, $C_\mu = 0.148$ (Fig. 7(b)), the power spectrum presents a dominant frequency 0.25 Hz. This is the subharmonic of the excitation frequency, indicating that the synthetic jet also has a prominent influence upon the wake vortex shedding. When increasing k to 2.00, C_μ to 0.850 (Fig. 7(e)), and k to 4.00, C_μ to 2.362 (Fig. 7(f)), the wake vortex shedding is all synchronized at the excitation frequency by the synthetic jet.

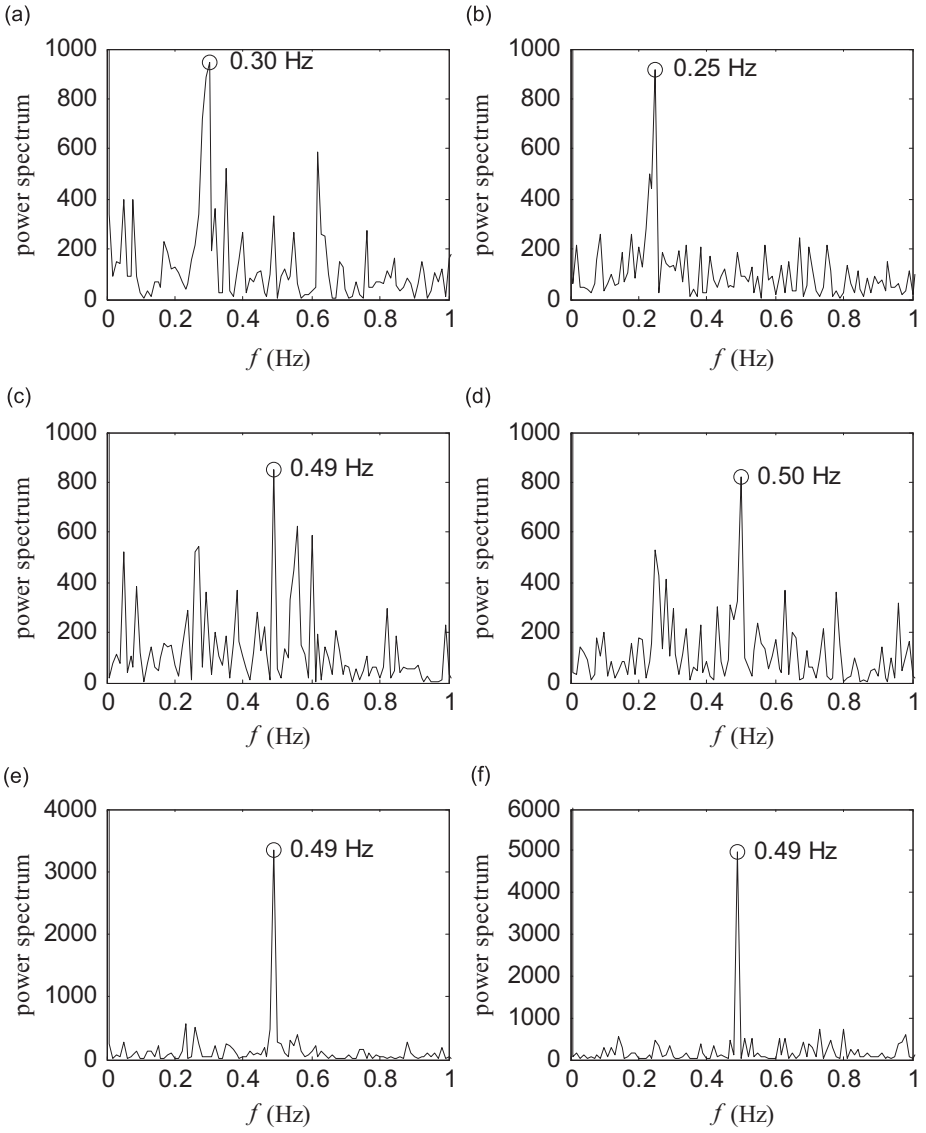

Fig. 7. Power spectrum of the spanwise vorticity $\omega_z D/U_\infty$ at $x/D = 3$, $y/D = 0.6$ for Re = 950: (a) natural; (b) $k = 0.25$, $C_\mu = 0.148$; (c) 0.50, 0.213; (d) 1.00, 0.378; (e) 2.00, 0.850; and (f) 4.00, 2.362.

The power spectrum at the representative position $x/D = 3$, $y/D = 0.6$ can well represent the frequency characteristic of the wake vortex shedding. Therefore, the primary power spectrum analysis indicates that when the excitation frequency is 1.67 times of the natural shedding frequency, the wake vortex in the near wake can be synchronized at the excitation frequency by the synthetic jet for $0.50 \leq k \leq 4.00$, $0.213 \leq C_\mu \leq 2.362$, while it is synchronized at the subharmonic excitation frequency for $k = 0.25$, $C_\mu = 0.148$. There are also other control methods that can result in vortex synchronization (Kim et al., 2009), which is also termed as vortex lock-on (Griffin and Hall, 1991), such as cylinder oscillations, including transverse oscillation (e.g., Blackburn and Henderson, 1999) and streamwise oscillation (e.g., Ongoren and Rockwell, 1988; Nishihara et al., 2005), and perturbations imposed on the free-stream, including transverse perturbations (e.g., Hall et al., 2003) and streamwise perturbations (e.g., Konstantinidis et al., 2003, 2005; Kim et al., 2006, 2009). According to these works, the occurrence of vortex synchronization is either due to the entrainment process of the cylinder motion (Blackburn and Henderson, 1999) or it could be generated when the incident mean flow has a sufficiently large periodic component superimposed upon it (Konstantinidis et al., 2003). Transverse oscillation and transverse perturbation flow may result in vortex synchronization at the excitation

frequency, while streamwise oscillation and streamwise perturbation flow may result in vortex synchronization at the subharmonic excitation frequency. However, under the present experimental condition, the occurrence of vortex synchronization is determined by the relative comparison of vortex strength between the synthetic jet and the wake vortex. The effect of the synthetic jet vortex pair on the wake shear layer is considered to play an important role in the occurrence of vortex synchronization. This will be further validated by the evolution of the vortex structures in the following.

3.3. Proper orthogonal decomposition (POD) analysis

Following Meyer et al. (2007), the POD analysis is applied to the velocity field including the streamwise and transverse velocities. Fig. 8 shows the percentage of the cumulative energy in POD modes to the total one for all cases. It is indicated that the energy percentage decreases as the mode becomes higher. The first few modes occupy most of the energy for all cases, since they represent the large-scale coherent structures which dominate the global flow field (Ma et al., 2003; Dipankar et al., 2007; Konstantinidis et al., 2007). For the controlled cases, the energy percentage is less than the natural case at the same mode. A probable explanation for this phenomenon is that the scale of the coherent structures dominating the flow filed for the controlled cases is smaller than the natural case.

Fig. 9 presents the first four POD modes of the vorticity field for all cases. They are calculated from the POD modes based on the velocity field. For the natural case, the first two modes contain more than 60% of the total energy. Fig. 9(a) shows the arrowhead structures with alternate sign symmetric about the x-axis, similar with a traveling wave. This traveling characteristic of the POD vorticity is due to the coupling of a pair of vortices that are shedding downstream out of phase during a period (Dipankar et al., 2007). Modes 3 and 4 are antisymmetric about the x-axis. The present first two POD patterns are in good agreement with those of Ma et al. (2000), Dipankar et al. (2007) and Konstantinidis et al. (2007). However, the higher modes are not completely identical in these results. According to Konstantinids et al. (2007), the symmetric distributions of the POD vorticity field with respect to the centerline represent antisymmetric vorticity fields, while those with mirrored symmetry represent symmetric ones. Therefore, the present modes 1 and 2 represent the essential antisymmetric shedding characteristic of the Karman vortex, while modes 3 and 4 represent the symmetric spatial background disturbances.

When the suction duty cycle factor k is $0.25 \leq k \leq 1.00$, i.e. the momentum coefficient C_μ is $0.148 \leq C_\mu \leq 0.378$ (Figs. 9(b)–(d)), distributions of the first two modes are similar with those of the natural case, indicating that the dominant antisymmetric vortex shedding mode does not change for these cases. However, the POD vorticity fields at higher modes 3 and 4 change evidently compared with the natural case. It is shown that two parallel rows of half-arrowhead structures with alternate sign are antisymmetric about the x-axis. Presumably, this characteristic is due

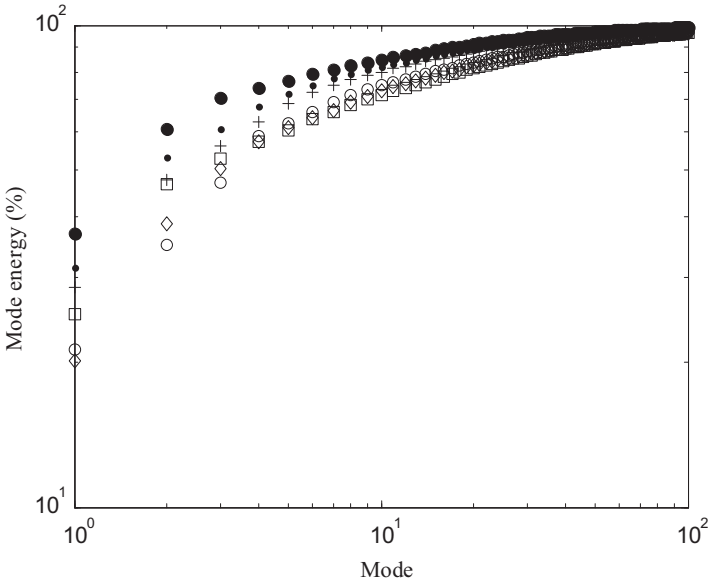

Fig. 8. Percentage of the cumulative POD modes energy to the total modes energy at Re = 950: ●, natural case; •, $k = 0.25$, $C_\mu = 0.148$; +, 0.50, 0.213; ○, 1.00, 0.378; ◇, 2.00, 0.850; and □, 4.00, 2.362.

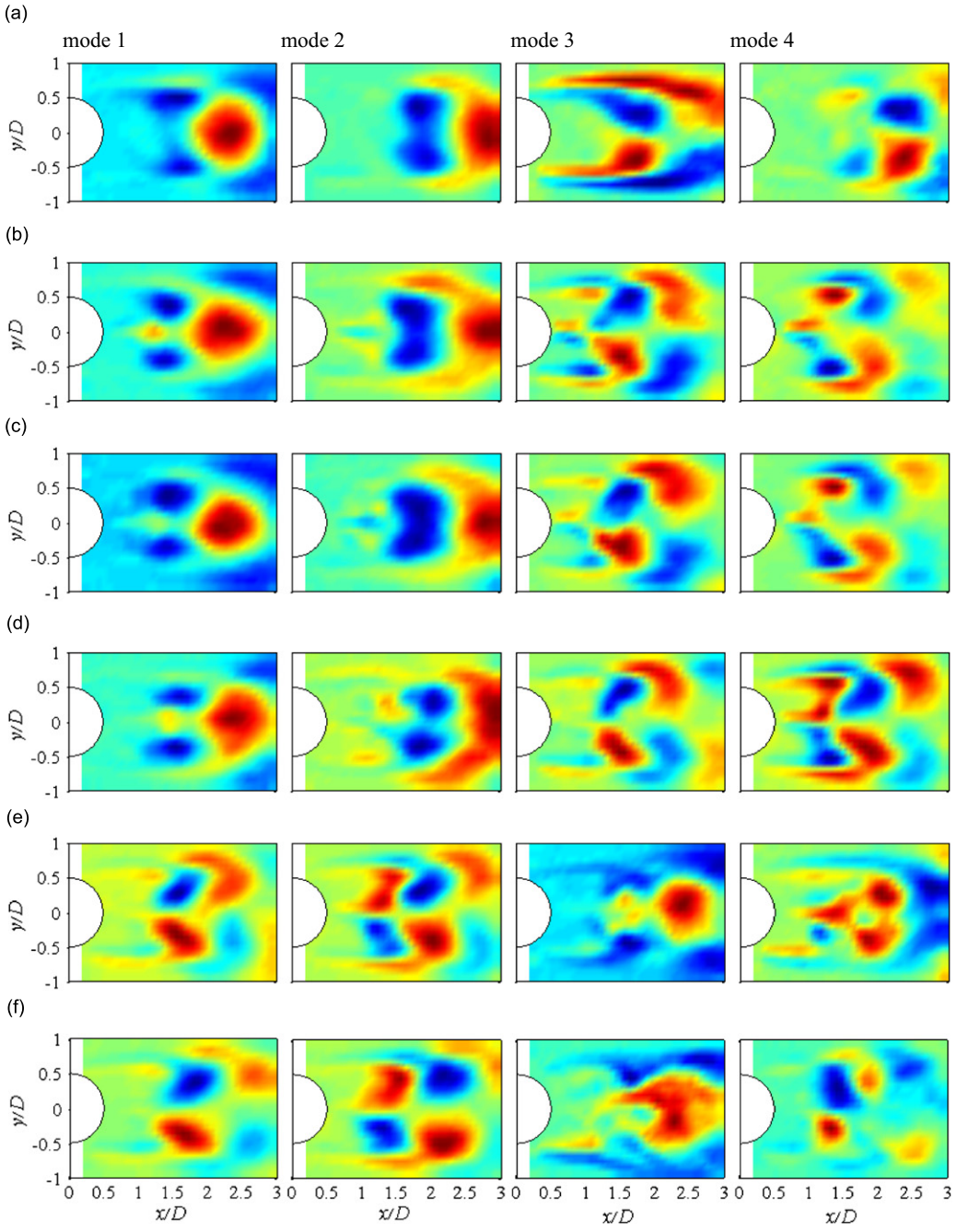

Fig. 9. POD modes of the vorticity field at Re = 950: (a) natural; (b) $k = 0.25$, $C_\mu = 0.148$; (c) 0.50, 0.213; (d) 1.00, 0.378; (e) 2.00, 0.850; and (f) 4.00, 2.362.

to the occurrence of the symmetric vortex shedding mode according to the distribution rule suggested by Konstantinids et al. (2007). It should reflect the characteristic of the synthetic jet flow field. Thus, it is suggested that the synthetic jet already has a significant influence on the flow around the circular cylinder. However, this influence is not strong enough to completely dominate the global flow field. Therefore, the inherent characteristic of the antisymmetric mode still dominates the wake vortex shedding.

For $2.00 \le k \le 4.00$, $0.850 \le C_\mu \le 2.362$ (Figs. 9(e) and (f)), the vortex strength of the synthetic jet is enhanced extremely. Thus the first two modes change essentially compared with the natural and $0.25 \le k \le 1.00$, $0.148 \le C_\mu \le 0.378$ cases. It is shown that two parallel rows of half-arrowhead structures with alternate sign are antisymmetric about the centerline, similar with those of modes 3 and 4 for cases $0.25 \le k \le 1.00$, $0.148 \le C_\mu \le 0.378$. Therefore, for $2.00 \le k \le 4.00$, $0.850 \le C_\mu \le 2.362$, the dominant vortex shedding mode is converted into a symmetric one, which will be further validated in the following. However, distributions of the higher modes are not so regular, indicating that they are also induced by uncertainties of the flow field.

3.4. Reconstruction of instantaneous spanwise vorticity

The global flow filed can be reconstructed by the selected POD modes. Ma et al. (2000), Konstantinidis et al. (2007) and Epps and Techet (2009) all indicated that only first two modes were needed to reconstruct the regular vortex shedding. However, we use the first four modes to reconstruct the spanwise vorticity field for all cases, since modes 3 and 4 represent the characteristic of the synthetic jet for the cases $0.25 \le k \le 1.00$, $0.148 \le C_\mu \le 0.378$.

3.4.1. $Re = 950$

Fig. 10(a) shows the antisymmetric shedding process of the instantaneous Karman vortex. Figs. 10(b)–(d) show the original spanwise vorticity filed at time $t_0+2\Delta t$, the corresponding first two modes and first 115 modes (corresponding to 99% of the total mode energy) reconstruction results, respectively. It is validated that using only the first two modes can well represent the original spanwise vorticity filed, while the reconstruction using higher modes can add more detail to the vorticity field and it will be more similar with the original pattern. However, the reconstruction result using the first four modes is enough to reveal the inherent characteristic of the flow field.

Fig. 11 shows the evolution of the instantaneous spanwise vorticity when adopting the standard actuator signal, namely $k = 1.00$, $C_\mu = 0.378$. For time $t_0+\Delta t$ to $t_0+3\Delta t$, within one period of the synthetic jet generation, the synthetic jet vortex pair interacts with the spanwise vorticity shear layers behind both sides of the circular cylinder as it convects downstream, resulting in the concentration of vorticities near the tails of the shear layers. Then the concentrated vorticities separate from the shear layers and roll up into vortex structures. Afterwards, the new induced wake vortices shed downstream with a nearly symmetric mode. This is similar with the results of Ongoren and Rockwell (1988), Liu and Fu (2003), Nishihara et al. (2005), Xu et al. (2006), Konstantinidis and Balabani (2007) and Jukes and Choi (2009b), who also found that the symmetric perturbations imposed on the cylinder wake might result in a modification of the vortex shedding mode from its natural antisymmetric one to a symmetric one. The present synthetic jet injects momentum downstream-wise from the rear stagnation point, which also imposes symmetric perturbations upon the flow over the circular cylinder. In the following period $t_0+T+\Delta t$ to $t_0+T+3\Delta t$, the synthetic jet vortex pair can also induce new wake vortices from both sides of the shear layers. However, the upper and lower induced wake vortices shed downstream out of phase.

Therefore, for the case of $k = 1.00$, $C_\mu = 0.378$, the wake vortex shedding mode varies between the symmetric mode and the antisymmetric one, since the strength of the synthetic jet vortex pair for this case is not strong enough to completely dominate the global flow field. When the synthetic jet vortex pair convects downstream, it also endures the effect of the vorticity shear layers behind both sides of the cylinder. The vorticity shear layers have an inherent instability that makes them shed downstream antisymmetrically. This antisymmetric instability may cause the deviation of the synthetic jet vortex pair from the centerline when convecting downstream sometimes, for example, towards lower side, resulting in the formation of the lower wake vortex developing and shedding downstream firstly, and then the upper wake vortex. However, the wake vortex is still synchronized at the excitation frequency by the synthetic jet vortex pair, according well with the power spectrum analysis in Fig. 7(d). Although the strength of the synthetic jet vortex pair for $k = 0.50$, $C_\mu = 0.213$ is reduced compared with that of $k = 1.00$, $C_\mu = 0.378$, the evolution of the wake vortex for both cases is similar. Therefore, it is not shown here.

Fig. 12 shows three-cycle evolution of the instantaneous spanwise vorticity for $k = 0.25$, $C_\mu = 0.148$. During the time t_0 to t_0+2T, the synthetic jet vortex pair has developed for two cycles, while it only induces one upper wake vortex that completely forms and sheds downstream. Similarly, during a latter two-cycle evolution of the synthetic jet vortex pair from t_0+T to t_0+3T, the lower wake vortex is induced and then sheds downstream. Therefore, in this case, the wake vortex is induced and completely generated due to the two-cycle effect of the synthetic jet vortex pair, validating the power spectrum analysis result of 0.25 Hz in Fig. 7(b). The induced wake vortex sheds downstream with an antisymmetric mode. Compared with the case of $k = 1.00$, $C_\mu = 0.378$, this is reasonable, since the synthetic jet vortex pair is attenuated greatly when decreasing k to 0.25, C_μ to 0.148. Thus its effect on the wake vortex is also weakened. However, the wake vortex shedding is synchronized at the subharmonic excitation frequency by the synthetic jet vortex.

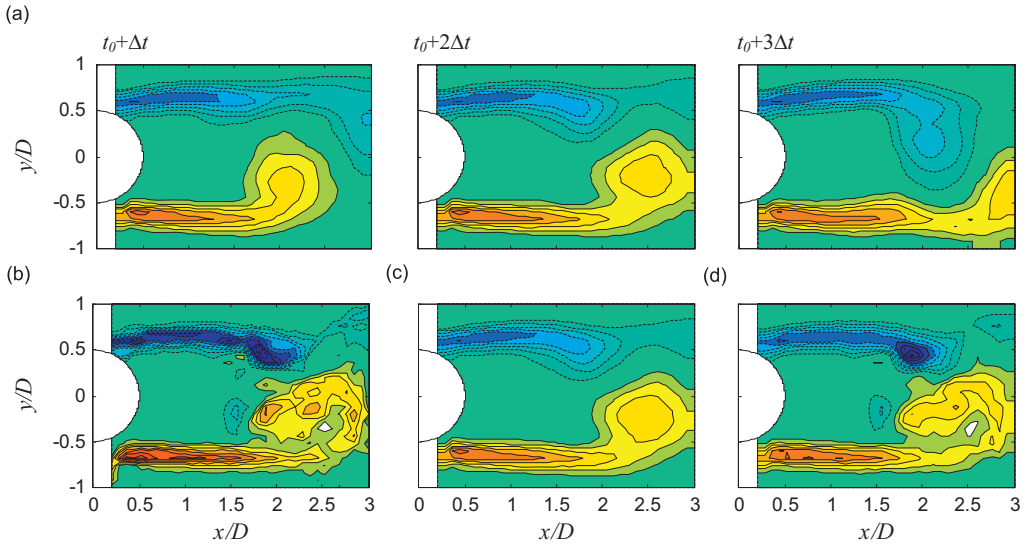

Fig. 10. Evolution of the instantaneous spanwise vorticity field for the natural case within one cycle at Re = 950: (a) vorticity reconstruction using first 4 modes, where t_0 is arbitrary and $\Delta t = 0.84$ s; (b) original spanwise vorticity field at time $t_0+2\Delta t$; (c) spanwise vorticity reconstruction using first 2 modes at time $t_0+2\Delta t$; and (d) spanwise vorticity reconstruction using first 115 modes (corresponding to 99% of the total mode energy) at time $t_0+2\Delta t$. Contour legends and contour levels are same as Fig. 4.

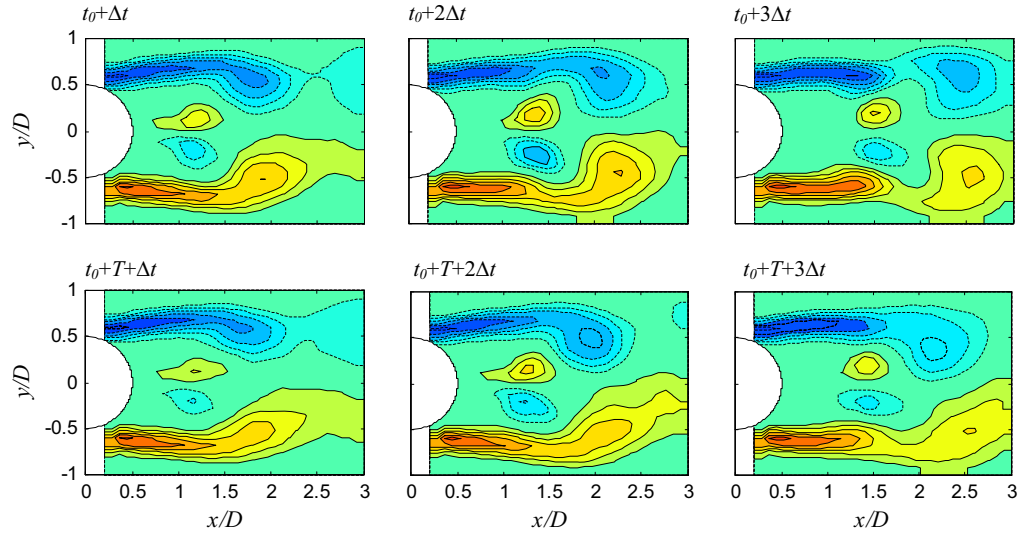

Fig. 11. Evolution of the instantaneous spanwise vorticity for $k = 1.00$, $C_\mu = 0.378$ within two cycles at Re = 950, where t_0 is the start of the blowing cycle, $T = 2.00$ s is the time duration of one cycle and $\Delta t = 0.50$ s. Contour legends and contour levels are same as Fig. 4.

For the case of $k = 2.00$, $C_\mu = 0.850$ (Fig. 13), the synthetic jet vortex pair becomes much stronger. The evolution of the synthetic jet vortex pair is not affected by the inherent instability of the antisymmetric wake vortex so much. On the contrary, the synthetic jet vortex can fully dominate the evolution of the wake vortex and make its shedding mode be converted into a symmetric one, while the antisymmetric shedding mode is rare to occur.

Increasing k to 4.00, C_μ to 2.362 (Fig. 14), the wake vortex is also synchronized at the excitation frequency by the synthetic jet vortex and its shedding mode is completely converted into a symmetric one. However, the formation

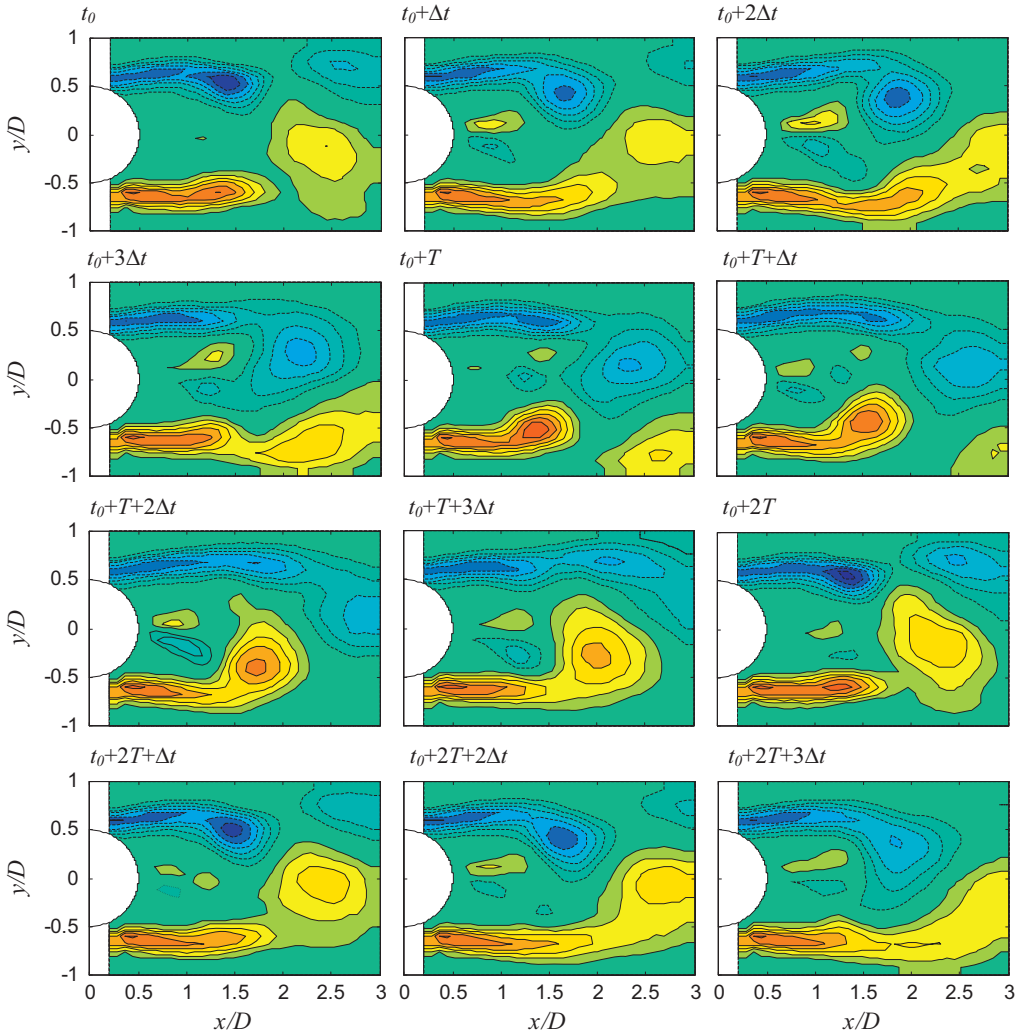

Fig. 12. Evolution of the instantaneous spanwise vorticity for $k = 0.25$, $C_\mu = 0.148$ within three cycles at Re = 950, where t_0 is the start of the blowing cycle, $T = 2.00$ s is the time duration of one cycle and $\Delta t = 0.50$ s. Contour legends and contour levels are same as Fig. 4.

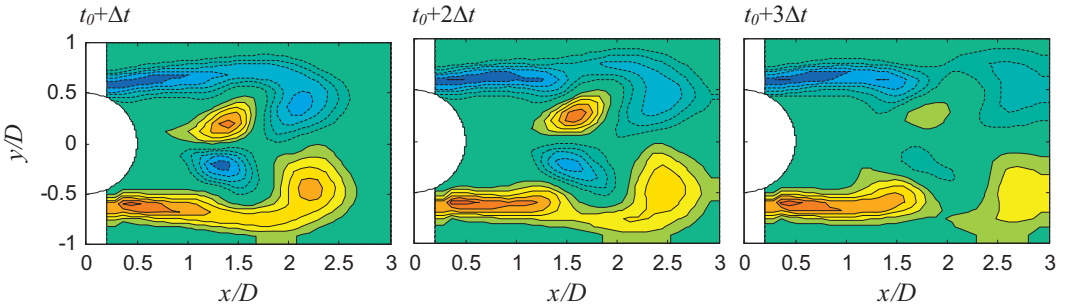

Fig. 13. Evolution of the instantaneous spanwise vorticity for $k = 2.00$, $C_\mu = 0.850$ within one cycle at Re = 950, where t_0 is the start of the blowing cycle, $T = 2.00$ s is the time duration of one cycle and $\Delta t = 0.50$ s. Contour legends and contour levels are same as Fig. 4.

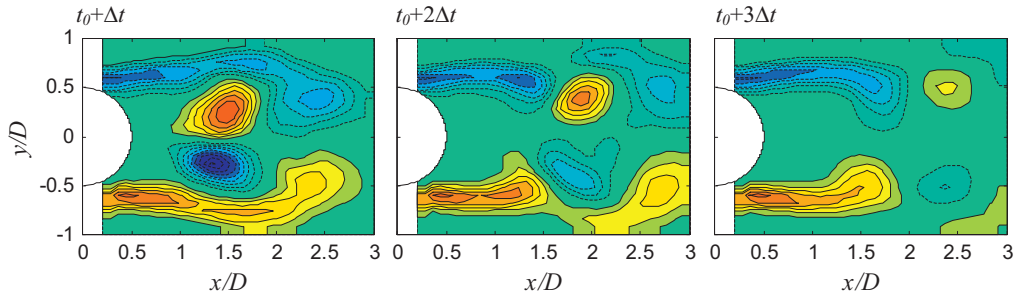

Fig. 14. Evolution of the instantaneous spanwise vorticity for $k = 4.00$, $C_\mu = 2.362$ within one cycle at Re = 950, where t_0 is the start of the blowing cycle, $T = 2.00$ s is the time duration of one cycle and $\Delta t = 0.50$ s. Contour legends and contour levels are same as Fig. 4.

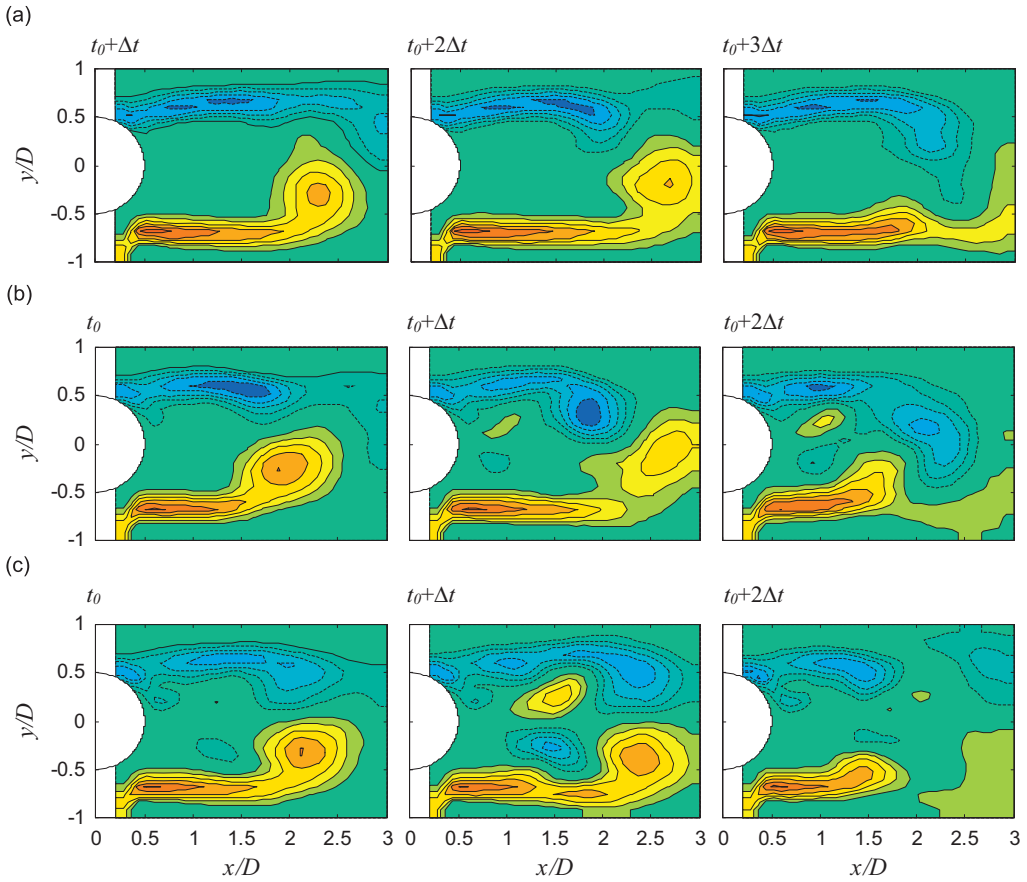

Fig. 15. Evolution of the instantaneous spanwise vorticity within one cycle at Re = 1600: (a) natural case, where t_0 is arbitrary and $\Delta t = 0.50$ s; (b) $k = 1.00$, $C_\mu = 0.129$, where t_0 is the start of the blowing cycle and $\Delta t = 0.50$ s; and (c) $k = 4.00$, $C_\mu = 0.807$, where t_0 is the start of the blowing cycle and $\Delta t = 0.50$ s. Contour legends and contour levels are same as Fig. 4.

time and length of the induced wake vortex are much shortened compared with the case of $k = 2.00$, $C_\mu = 0.850$, since the synthetic jet vortex is enhanced extremely in this case.

3.4.2. *Re = 1600*

The enhancement of the control effect using the novel synthetic jet can also be validated at a higher Reynolds number Re = 1600. Note that the lack of vorticity patterns just under the lower side of the circular cylinder in Fig. 15 is due to

the shadow of the cylinder when illuminating the flow field. Fig. 15(a) shows the antisymmetric shedding process of the Karman vortex within one period, corresponding to the natural shedding frequency 0.50 Hz. When the synthetic jet works at 0.50 Hz using the standard actuator signal, namely $k = 1.00$, $C_\mu = 0.129$ (Fig. 15(b)), the synthetic jet vortex pair has a limited influence on the evolution of the wake vortex. It still sheds downstream with an antisymmetric mode and the shedding frequency is also 0.50 Hz. However, when increasing k to 4.00, C_μ to 0.807 (Fig. 15(c)), the wake vortex shedding is converted into a symmetric mode due to the enhanced influence of the synthetic jet vortex pair, indicating that the synthetic jet could fully synchronize the wake vortex. It is in the vicinity of the cases $0.850 \leq C_\mu \leq 2.362$ at $\mathrm{Re} = 950$, where the symmetric shedding mode also occurs.

Note that for the same excitation frequency and suction duty cycle factor, the strength of the synthetic jet vortex pair at $\mathrm{Re} = 1600$ is less than that at $\mathrm{Re} = 950$, since the momentum coefficient is much lower for the former case, such as the comparisons between Fig. 15(b) and Fig. 11, Fig. 15(c) and Fig. 14. In addition, the strength of the wake vortex at a higher Reynolds number is much stronger. Thus its attenuation effect upon the synthetic jet vortex pair is enhanced. Therefore, the control effect of the synthetic jet vortex pair upon the flow around the circular cylinder is reduced as the Reynolds number based on the cylinder diameter increases. However, it can still be enhanced by increasing the suction duty cycle factor even at the same excitation frequency.

3.5. Comparison between phase-averaging and POD techniques

The phase-averaging technique can eliminate the small-scale turbulent structures and background disturbances in order to extract the dominant large-scale coherent structures from the flow field. However, it should be careful when performing the phase average of the global field. Comparing the instantaneous reconstruction spanwise vorticity (Figs. 11–14) with the phase-averaged spanwise vorticity (Fig. 4), it is indicated that, when the wake vortex is synchronized by the synthetic jet and the shedding mode is completely converted into a symmetric one, the phase-averaged spanwise vorticity is in good agreement with the instantaneous reconstruction result, suggesting that the phase-averaged patterns do not vary along with the position of the selected phase-averaging reference signal. However, when the synthetic jet could not dominate the wake vortex completely, the phase-averaged result based on the rear stagnation point could not reflect the characteristics of the wake vortex shedding. In order to present the characteristics of wake vortex shedding, the phase-averaging reference signal should be selected at a further downstream position. In one word, the phase-averaged result varies based on different reference signals. Thus the POD method is useful, especially when there is lack of overall understanding of the global flow field while evolution of the instantaneous flow filed should be analyzed.

4. Conclusions

Flow around a circular cylinder is controlled by a synthetic jet positioned at the rear stagnation point using a novel synthetic jet. The suction duty cycle factor k, defined as the ratio between the time duration of the suction cycle and the blowing cycle, is used as the parameter to characterize the novel synthetic jet signal. Meanwhile, the equivalent momentum coefficient C_μ is introduced as the determining parameter for comparison between the synthetic jet output and the oncoming flow. It is indicated that, when increasing the suction duty cycle factor, the momentum coefficient is also enhanced, and a stronger and larger scale synthetic jet vortex pair is generated and it can reach further downstream. This characteristic has a significant influence on the wake vortex shedding of the circular cylinder.

In order to extract the dominant wake vortex shedding mode from the background disturbances, the proper orthogonal decomposition (POD) technique is applied for the analysis of the spanwise vorticity field. It is indicated that the synthetic jet vortex pair induced near the exit convects downstream and interacts with the spanwise vorticity shear layers behind both sides of the circular cylinder, resulting in the concentration of vorticities near the tails of the shear layers. Then the concentrated vorticities separate from the shear layers and roll up into vortex structures. When increasing the suction duty cycle factor, namely the momentum coefficient, the evolution patterns of the wake vortex can be categorized into three groups at $\mathrm{Re} = 950$. For $k = 0.25$, $C_\mu = 0.148$, vortex synchronization at the subharmonic excitation frequency occurs and the wake vortex shedding mode is the antisymmetric one. For $0.50 \leq k \leq 1.00$, $0.213 \leq C_\mu \leq 0.378$, vortex synchronization at the excitation frequency occurs, and the wake vortex shedding mode varies between the symmetric and antisymmetric shedding modes. For $2.00 \leq k \leq 4.00$, $0.850 \leq C_\mu \leq 2.362$, vortex synchronization at the excitation frequency occurs, and the wake vortex shedding mode is completely converted into a symmetric one. Therefore, the control effect of the synthetic jet upon the flow around a circular cylinder can be enhanced by increasing the suction duty cycle factor of the actuator signal so as to increase the momentum coefficient.

It is also noteworthy that the momentum coefficient in the present work is much higher than the previous ones with the synthetic jet positioned near the separation point (Amitay et al., 1997, 1998; Tensi et al., 2002). This can be attributed to the different control mechanisms between these two arrangements. For the latter case, the perturbations can interact with the shear layer directly through the Kelvin–Helmholtz instability and usually a small perturbation with the natural shedding frequency or its harmonic may trigger the global variations of the wake vortex. For the former case, the localized perturbations interact with the wake shear layers though the rear recirculation region, which is much like another control method base bleed (Fu and Rockwell, 2005; Baek and Karniadakis, 2009). Thus, the strength of the synthetic jet vortex must not be too small to avoid being attenuated in the rear recirculation region before interacting with the wake vortex shear layers. Therefore, the present momentum coefficient must be much higher than the previous investigations. However, it is also indicated that the momentum coefficient can be enhanced extremely by increasing the suction duty cycle factor, while other parameters are kept unchanged. This is very useful for the engineering applications of the synthetic jet when high momentum is usually needed.

Acknowledgement

This work has been supported by the National Natural Science Foundation of China (No. 10832001) and No. 50976007.

References

Abdou, S., Ziada, S., 2006. Spanwise characteristics of high-aspect-ratio synthetic jets. AIAA Journal 44, 1516–1523.

Amitay, M., Honohan, A., Trautman, M., Glezer, A., 1997. Modification of the aerodynamic characteristics of bluff bodies using fluidic actuators. AIAA Paper, 97-2004.

Amitay, M., Smith, B.L., Glezer, A., 1998. Aerodynamic flow control using synthetic jet technology. AIAA Paper, 98-0208.

Baek, H., Karniadakis, G.E., 2009. Suppressing vortex-induced vibrations via passive means. Journal of Fluids and Structures 25, 848–866.

Berkooz, G., Holmes, P., Lumley, J.L., 1993. The proper orthogonal decomposition in the analysis of turbulent flows. Annual Review of Fluid Mechanics 25, 539–575.

Béra, J.C., Michard, M., Sunyach, M., Comte-Bellot, G., 2000. Changing lift and drag by jet oscillation: experiments on a circular cylinder with turbulent separation. European Journal of Mechanics B: Fluids 19, 575–595.

Blackburn, H.M., Henderson, R.D., 1999. A study of two-dimensional flow past an oscillating cylinder. Journal of Fluid Mechanics 385, 255–286.

Cantwell, B., Coles, D., 1983. An experimental study of entrainment and transport in the turbulent near wake of a circular cylinder. Journal of Fluid Mechanics 136, 321–374.

Choi, H., Jeon, W.P., Kim, J., 2008. Control of flow over a bluff body. Annual Review of Fluid Mechanics 40, 113–139.

Crook, A., Sadri, A.M., Wood, N.J., 1999. The development and implementation of synthetic jets for the control of separated flow. AIAA Paper, 99-3176.

Dipankar, A., Sengupta, T.K., Talla, S.B., 2007. Suppression of vortex shedding behind a circular cylinder by another control cylinder at low Reynolds numbers. Journal of Fluid Mechanics 573, 171–190.

Epps, B., Techet, A.H., 2009. An error threshold criterion for singular value decomposition modes extracted from PIV data. Experiments in Fluids 48, 355–367.

Feng, L.H., Wang, J.J., Xu, C.J., 2008. Experimental verification of a novel actuator signal for efficient synthetic jet. Journal of Experiments in Fluid Mechanics 22, 6–10 (in Chinese).

Fu, H., Rockwell, D., 2005. Shallow flow past a cylinder: control of the near wake. Journal of Fluid Mechanics 539, 1–24.

Fujisawa, N., Takeda, G., 2003. Flow control around a circular cylinder by internal acoustic excitation. Journal of Fluids and Structures 17, 903–913.

Fujisawa, N., Takeda, G., Ike, N., 2004. Phase-averaged characteristics of flow around a circular cylinder under acoustic excitation control. Journal of Fluids and Structures 19, 159–170.

Glezer, A., Amitay, M., 2002. Synthetic jets. Annual Review of Fluid Mechanics 34, 503–529.

Glezer, A., Amitay, M., Honohan, A.M., 2003. Aspects of low- and high-frequency aerodynamic flow control. AIAA Paper, 2003-0533.

Griffin, O.M., Hall, M.S., 1991. Review—vortex shedding lock-on and flow control in bluff body wakes. ASME Journal of Fluids Engineering 113, 526–537.

Hall, J.W., Ziada, S., Weaver, D.S., 2003. Vortex-shedding from single and tandem cylinders in the presence of applied sound. Journal of Fluids and Structures 18, 741–758.

Hilberg, D., Lazik, W., Fiedler, H.E., 1994. The application of classical POD and snapshot POD in a turbulent shear layer with periodic structures. Applied Scientific Research 53, 283–290.

Holman, R., Utturkar, Y., Mittal, R., Smith, B.L., Cattafesta, L., 2005. Formation criterion for synthetic jets. AIAA Journal 43, 2110–2116.

Ingard, U., Labate, S., 1950. Acoustic circulation effects and the nonlinear impedance of orifices. Journal of the Acoustical Society of America 22, 211–218.

Jukes, T.N., Choi, K.S., 2009a. Long lasting modifications to vortex shedding using a short plasma excitation. Physical Review Letters 102, 254501.
Jukes, T.N., Choi, K.S., 2009b. Flow control around a circular cylinder using pulsed dielectric barrier discharge surface plasma. Physics of Fluids 21, 084103.
Kim, W., Yoo, J.Y., Sung, J., 2006. Dynamics of vortex lock-on in a perturbed cylinder wake. Physics of Fluids 18, 074103.
Kim, S.H., Park, J.Y., Park, N., Bae, J.H., Yoo, J.Y., 2009. Direct numerical simulation of vortex synchronization due to small perturbations. Journal of Fluid Mechanics 634, 61–90.
Konstantinidis, E., Balabani, S., 2007. Symmetric vortex shedding in the near wake of a circular cylinder due to streamwise perturbations. Journal of Fluids and Structures 23, 1047–1063.
Konstantinidis, E., Balabani, S., Yianneskis, M., 2003. The effect of flow perturbations on the near wake characteristics of a circular cylinder. Journal of Fluids and Structures 18, 367–386.
Konstantinidis, E., Balabani, S., Yianneskis, M., 2005. The timing of vortex shedding in a cylinder wake imposed by periodic inflow perturbations. Journal of Fluid Mechanics 543, 45–55.
Konstantinidis, E., Balabani, S., Yianneskis, M., 2007. Bimodal vortex shedding in a perturbed cylinder wake. Physics of Fluids 19, 011701.
Liu, S., Fu, S., 2003. Regimes of vortex shedding from an in-line oscillating circular cylinder in the uniform flow. Acta Mechanica Sinica 19, 118–126.
Lucor, D., Karniadakis, G.E., 2004. Noisy inflows cause a shedding-mode switching in flow past an oscillating cylinder. Physical Review Letters 92, 154501.
Ma, X., Karamanos, G.S., Karniadakis, G.E., 2000. Dynamics and low-dimensionality of a turbulent near wake. Journal of Fluid Mechanics 410, 29–65.
Ma, X., Karniadakis, G.E., Park, H., Gharib, M., 2003. DPIV-driven flow simulation: a new computational paradigm. Proceedings of the Royal Society of London Series A 459, 547–565.
Meyer, K.E., Pedersen, J.M., Oktayözcan, 2007. A turbulent jet in crossflow analysed with proper orthogonal decomposition. Journal of Fluid Mechanics 583, 199–227.
Nishihara, T., Kaneko, S., Watanabe, T., 2005. Characteristics of fluid dynamic forces acting on a circular cylinder oscillated in the streamwise direction and its wake patterns. Journal of Fluids and Structures 20, 505–518.
Ongoren, A., Rockwell, D., 1988. Flow structure from an oscillating cylinder. Part 2. Mode competition in the near wake. Journal of Fluid Mechanics 191, 225–245.
Smith, B.L., Glezer, A., 1998. The formation and evolution of synthetic jets. Physics of Fluids 10, 2281–2297.
Shan, R.Q., Wang, J.J., 2010. Experimental studies of the influence of parameters on axisymmetric synthetic jets. Sensors and Actuators A: Physical 157, 107–112.
Shuster, J.M., Smith, D.R., 2004. A study of the formation and scaling of a synthetic jet. AIAA Paper, 2004-0090.
Sung, J., Yoo, J.Y., 2003. Near-wake vortex motions behind a circular cylinder at low Reynolds number. Journal of Fluids and Structures 17, 261–274.
Tensi, J., Boué, I., Paillé, F., Dury, G., 2002. Modification of the wake behind a circular cylinder by using synthetic jets. Journal of Visualization 5, 37–44.
Wang, J.J., Feng, L.H., Xu, C.J., 2007. Experimental investigations on separation control and flow structure around a circular cylinder with synthetic jet. Science in China E: Technological Sciences 50, 550–559.
Wolfe, D., Ziada, S., 2003. Feedback control of vortex shedding from two tandem cylinders. Journal of Fluids and Structures 17, 579–592.
Xu, S.J., Zhou, Y., Wang, M.H., 2006. A symmetric binary-vortex street behind a longitudinally oscillating cylinder. Journal of Fluid Mechanics 556, 27–43.
Zhang, P.F., Wang, J.J., 2007. Novel signal wave pattern for efficient synthetic jet generation. AIAA Journal 45, 1058–1065.
Zhang, P.F., Wang, J.J., Feng, L.H., 2008. Review of zero-net-mass-flux jet and its application in separation flow control. Science in China E: Technological Sciences 51, 1315–1344.
Zhou, Y., Yiu, M.W., 2006. Flow structure, momentum and heat transport in a two-tandem-cylinder wake. Journal of Fluid Mechanics 548, 17–48.
Ziada, S., 1995. Feedback control of globally unstable flows: impinging shear flows. Journal of Fluids and Structures 9, 907–923.